Phys. Status Solidi A **210**, No. 5, 994–999 (2013) / **DOI** 10.1002/pssa.201200798

Part of Special Section on
Engineering of Functional Interfaces

physica status solidi a
www.pss-a.com
applications and materials science

Copper–zinc thin films reactively co-sputtered from a two-component sectioned cathode

Wolfgang Burgstaller, Andrei Ionut Mardare, and Achim Walter Hassel*

Institute for Chemical Technology of Inorganic Materials, Johannes Kepler University Linz, Altenberger Str. 69, 4040 Linz, Austria

Received 5 October 2012, revised 15 February 2013, accepted 18 February 2013
Published online 29 April 2013

Keywords combinatorial libraries, co-sputter deposition, Cu–Zn thin film alloys, two-component sectioned cathode

* Corresponding author: e-mail achimwalter.hassel@jku.at, Phone: +43 732 2468 8700, Fax: +43 732 2468 8905

Cu–Zn thin film oxide alloys have been fabricated by reactive co-sputter deposition using a sectioned two-component metallic target. A Cu–Zn compositional spread ranging from Cu–88 at.% Zn to Cu–1.3 at.% Zn defining a combinatorial library was identified. A thickness gradient with a maximum of 4.1 μm was found. The microstructure of the Cu–Zn oxide thin films was analyzed by SEM, finding three compositional zones with structural differences. XRD investigations have revealed different crystalline structures for each of the three zones. CuZn intermetallics and pure Cu-phase were identified together with Cu_2O and ZnO. For the first compositional zone XPS depth profiles have shown metallic phase segregation at the thin film/substrate interface. At Zn concentrations higher than 45 at.% Zn an increased tendency of ZnO formation was identified.

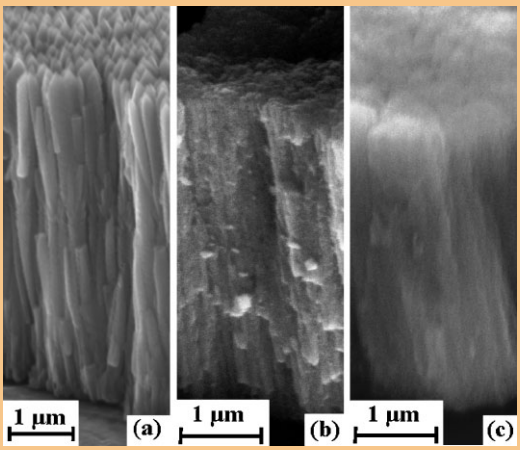

1 Introduction Among various deposition methods, sputtering plays a crucial role due to the tunability of the final film properties. Several parameters (e.g. substrate temperature, angle of incidence, etc.) can easily be changed during the sputtering process in order to ensure the thin film growth according to a chosen structure zone model [1]. This idea was already exploited when investigating Cu and Zn thin films deposited on both glass and stainless steel substrates and a clear dependence of the growth model on the deposition conditions was established [2]. Apart from the metallic Cu and Zn films, their oxides also present scientific interest.

In recent years, ZnO thin films have gained drastically increased interest and were thoroughly investigated due to their excellent properties for use as semiconducting, photoconducting, piezoelectric, optical waveguide, and transparent electrode materials [3]. The amount of oxygen in an Ar/O_2 plasma can strongly affect the ZnO properties, such as transparency and conductivity [4]. Both, DC and RF reactive sputtering techniques produce high quality thin films for a wide range of applications [5]. In transparent electronics, ZnO plays an important role not only due to its high transparency in both visible and near infrared but also due to its large exciton binding energy, forming a layered structure at low temperatures [6]. Upon doping, ZnO is largely used for sensors and actuators [7]. When deposited on Cu-metallized Si-wafers, the characteristics of ZnO depend on the nature of the Cu layers [8].

A great scientific attention is given to Cu_2O thin films deposited by sputtering due to their industrial applications such as thermal insulation, high hardness, optical nonlinearity, and low friction materials [9]. In either DC or RF sputtering techniques, Cu_2O thin films are easily obtained

and their microstructure is strongly affected by the oxygen partial pressure used during the deposition [10, 11].

In combination with ZnO, Cu is used for doping purposes due to improved optical [12] and electrical properties [13]. The microstructure of Cu-doped ZnO thin films depends not only on the deposition parameters, but also on the total thickness of the films [14]. The photoluminescence of such a material is greatly exploited in the semiconductor industry for light emitters, varistors, transparent high power electronics, etc. [15]. The nanocrystallinity obtained in Cu–ZnO thin films can for example be tuned for being used in CO sensing applications [16].

The formation of thin film combinatorial libraries is of high interest due to the possibility of finding materials having specific properties related to a certain composition [17–20].

Glow discharge sputtering from two-component cathode target was already employed for the co-deposition of Cu and Zn metallic thin films [21]. In the present work, a two-component sectioned cathode is used for reactive co-deposition of ZnO and Cu_2O in order to study the basic growth of Cu–Zn oxide thin film combinatorial libraries.

2 Experimental The Cu–Zn thin film oxide alloys were produced using a reactive co-sputter deposition technique involving a single target. A high purity copper disc (>99.99 at.%) with a diameter of 50 mm was used as a template for the fabrication of the two-component sectioned cathode. The surface of the disc was ground using SiC grinding paper with grain sizes down to 4000. A high purity Zn plate (>99.99 at.%) in the shape of a half disc, 0.9 mm in thickness, was machined to match the diameter of the Cu disc. Its surface was polished in the same manner to comply with the requests for the target. The Zn half-disc was fixed to the surface of the Cu disc so that their diameters coincided. In this way, both materials have the same exposed area. Electrical contacting between the Cu and Zn plates was achieved by using highly conductive silver suspension. This also provided good mechanical adhesion between the parts upon pressing and drying of the silver paste for 2 h at 50 °C. Extra care was taken when fixing both materials together so that in the vicinity of the edge of the Zn half-disc, no silver could leak out from the interface. The obtained Cu–Zn two-component cathode was used for deposition of Cu–Zn thin film oxide alloys. In Fig. 1a the photograph of the Cu–Zn sectioned cathode is presented and in Fig. 1b the as-deposited film is shown.

For the reactive sputtering process, the two-component target was mounted in a commercial DC sputtering system (Hummer II from Technics, USA) with a substrate–target distance of 17 mm, which was kept constant during the entire deposition process. This short deposition distance was chosen in order to maximize the individual thickness gradients produced by each metal due to their cosine laws of evaporation. It must be emphasized that this is intentionally chosen, since the attempt was to create a sufficiently steep gradient. The necessary vacuum was ensured inside the vacuum chamber by an integrated pumping unit (Direct

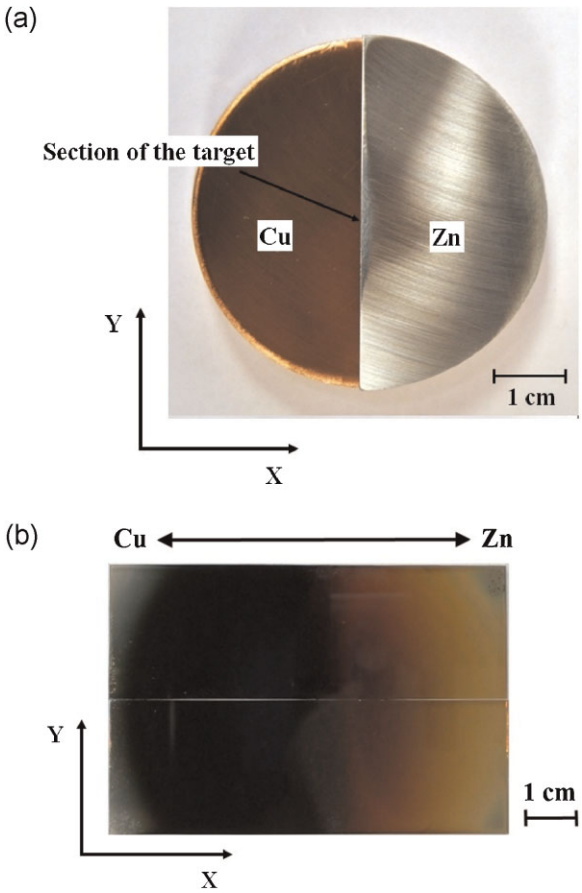

Figure 1 (a) Two-component sectioned metallic Cu–Zn target. (b) Photograph of the as-deposited film on a double glass substrate.

Torr) able to provide a base pressure of down to 10 Pa. At this pressure equilibrium is reached, the residual gas mixture having a partial oxygen pressure of 2.1 Pa. This partial pressure provided the necessary reactivity for oxide formation during deposition. High purity (5.0) Ar-gas flow (0.042 sccm) was used for obtaining a deposition pressure of 35 Pa which in turn has decreased the oxygen partial pressure to 0.6 Pa. This value can be considered constant during the deposition process, due to the natural leaks of the chamber responsible for the initial base pressure. Before each deposition, the chamber was purged at least three times with Ar for ensuring a sufficient reduction of residual gases adsorbed to the inner surfaces. The electrical field necessary for igniting the plasma was achieved using a 1.2 kV DC power source. During deposition, currents as high as 30 mA were recorded for a power of approximately 30 W. A deposition rate of approximately 0.1 nm s^{-1} was used during the vapour phase formation of the Cu–Zn thin film oxide alloys. This had as a result the obtaining of maximum 4.1 μm thick films. During the sputtering process, the anode was an Al disc also serving as sample holder. Two borosilicate glass slides (26 mm × 76 mm) were simultaneously used as substrates for the Cu–Zn thin film deposition at room temperature. In this way an almost square joint substrate surface was obtained.

The compositional spread of the Cu–Zn thin film oxide alloys was investigated with spatial resolution using a X-Strata 980-A scanning X-ray fluorescence spectrometer (SXRF) from Oxford Instruments. The microstructure analysis of the Cu–Zn combinatorial library was carried out using a field emission Zeiss Gemini 1540 XB SEM with 20 kV acceleration voltage and in-lens detection at a working distance of 9 mm. Additionally, EDX analysis (Oxford INCA) was performed at distinct locations for a precise correlation to the SEM imaging and to the SXRF data. The surface microstructure of the Cu–Zn compositional spread was imaged employing a Nanosurf Easyscan 2 AFM operating in contact mode, equipped with a CONTR-Si-cantilever. Crystallographic analysis was performed using an X'Pert Pro PW 3040/60 XRD system (Philips) equipped with a Cu tube (45 kV, 40 mA) and X'Celerator RTMS detector. The in-depth compositional analysis of the Cu–Zn thin film oxide alloys was performed using XPS depth profiling (Thermo Fischer – Theta Probe).

3 Results and discussion Generally, in any co-deposition from vapour phase a compositional gradient is expected to be found on the substrate surface. This is due to the cosine law [22] governing the thickness distribution across the substrate. When two or more materials are simultaneously sputtered from different targets, each material may in principle produce its own thickness distribution. In the simplest case of two materials, the two opposing thickness gradients will result in a uniaxial compositional spread across the substrate.

In order to investigate the compositional gradients obtained during the co-sputtering of Cu and Zn from the two-component sectioned cathode, XRF analysis was performed while scanning the substrate surface (spot size 0.1 mm). In this way, a direct correlation between the Cu–Zn thin films composition and the substrate geometry could be obtained. In Fig. 2 such a compositional mapping is presented as a 3D surface. The axes presented in the horizontal plane describe the physical dimension of both joint glass substrates. On the vertical axis the Cu content is plotted using a color code for the entire analyzed surface. The Zn concentration is complementary to the Cu scale. At the substrate edge placed directly under the Cu half-cathode, a Cu concentration reaching 98.7 at.% was found, while on the opposite side of the substrate directly under the Zn half-target a Zn concentration of 87.7 at.% was measured. This defines an overall compositional gradient of 86.4 at.% and a compositional resolution of 1.92 at.% mm^{-1}. However, an almost linear compositional gradient can be observed only in the central region of the substrate approximately ranging from 15 to 35 mm on the x-axis. In the direction perpendicular to the compositional Cu–Zn gradient, a compositional conservation can be observed as seen by the almost parallel colored regions corresponding to various compositions. This is to be expected due to the large area of the two-component sectioned target.

A side effect of using a short substrate–target distance is represented by an overall Cu–Zn thin film thickness gradient. This gradient was automatically obtained during the XRF compositional scan by analyzing the peak heights of the triangular peaks in the fluorescence spectra. In Fig. 3 the Cu–Zn thin film oxide alloy thickness distribution is plotted in colour coded 3D graph as measured over the entire joint substrate surface. A parabolic surface can be observed with a maximum peak value of 4.1 μm located in the mid plane perpendicular (y-axis) to the section of the two-component target. However, on the plane containing the section of the two-component cathode a shift of the maximum of the thickness distribution towards the Cu side was noticed. Most likely this shift appears due to the scattering of atoms occurring at the step formed by the geometry of the Zn half-disc in the target section plane. Starting from the peak of the parabolic distribution, the thickness of the Cu–Zn thin films decreases fast in the direction normal to the section of the cathode, the lowest value of approximately 500 nm being observable at the edges of the joint substrate. In the direction

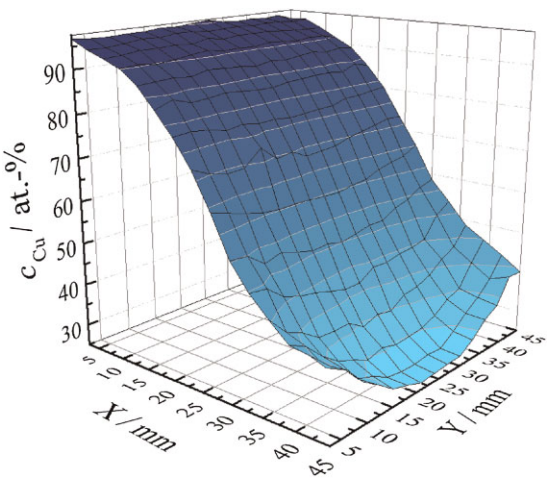

Figure 2 Scanning XRF analysis map of the Cu–Zn thin film oxide alloys obtained by sectioned target co-sputter deposition.

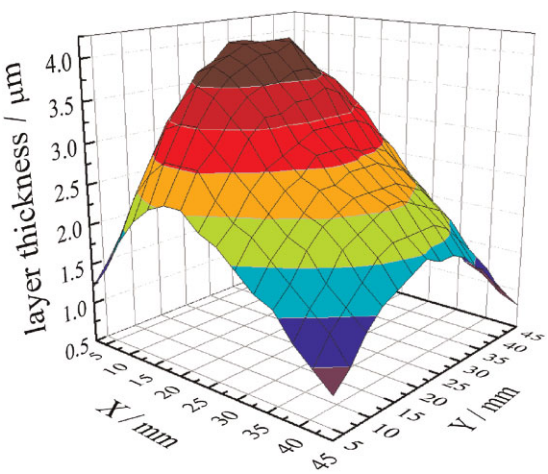

Figure 3 Distribution of the Cu–Zn thin film oxide alloy thickness with respect to the position on the sample.

parallel to the two-component target section a weaker thickness gradient can also be observed. This is due to the weakening of the sputter yield at the edges of the cathode.

The microstructure of the Cu–Zn thin film combinatorial library was analyzed by SEM at various compositions. A tableau, containing surface details imaged at several locations across the substrate is presented in Fig. 4. Each position on this library corresponds to a different alloy for which the composition is given as an inlet in the images of Fig. 4. The composition of each investigated alloy is given for the corresponding position. At high Cu concentrations (e.g., Cu–1.3 at.% Zn) a fine grained structure with tetrahedral grains smaller than 100 nm is found (zone I). Increasing the amount of Zn in the compositional spread had as a first result an increase of the grain sizes. This grain evolution is clearly observed for Zn concentrations up to 5.8 at.% where the grain sizes are approaching 200 nm while conserving their shape. From this point on, a second compositional zone (II) can be defined where the grain sizes do not substantially change but their shape starts to be influenced by the increasing Zn content. For Cu–16 at.% Zn a flattened surface with rounded grains can already be observed with still clearly visible grain boundaries. Similar results have been found in previous reports [5, 8]. After the geometry of the microstructure changed from tetrahedral to round grains during the transition from the first to the second compositional zone, a new increase of the grain sizes was observed reaching approximately 700 nm for Cu–39 at.% Zn. A further increase of the Zn concentration had as a result the observation of a third compositional zone (III) starting approximately at Cu–45 at.% Zn, where the microstructure changes once more. The newly observed surfaces show small compact grains with sizes of approximately 150 nm as visible in Fig. 4 for Cu–55.6 at.% Zn.

AFM measurements showed a gradient in surface roughness ranging from $R_{RMS} = 11.1$ nm starting at the Cu rich composition of the alloy to $R_{RMS} = 16.6$ nm found for the Zn dominated phases.

In order to study the morphology of the Cu–Zn thin film oxide alloys, cross-section imaging by SEM was used. In Fig. 5 representative cross-sections characteristic for each compositional zone previously identified are shown. In the first zone (Fig. 5a) at high Cu concentrations (Cu–1.5 at.% Zn) a columnar structure terminated with tetrahedral tips can be clearly identified. The sharp grain boundaries observed on the surface of the first zone in Fig. 4 are also clearly defined in depth of the Cu–Zn thin films reaching the substrate interface. At higher Zn concentrations in the second compositional zone, the columnar structure is still visible (Fig. 5b) at Cu–25 at.% Zn. However, the shape change of the surface grains is connected to a certain level of columnar compression within the Cu–Zn thin films. The cross-section does not show clear boundaries between columns which can explain the more compact surface observed in the second compositional zone in Fig. 4. The highest amount of Zn present in the Cu–Zn thin film compositional spread is related to a further surface compacting observable also in the cross-sections from the third compositional zone. In Fig. 5c

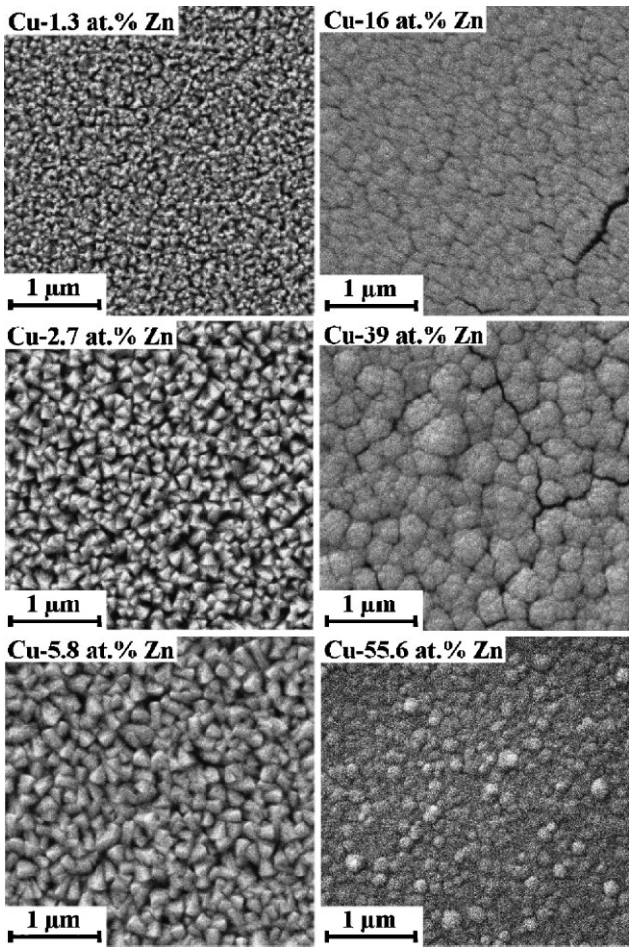

Figure 4 SEM image of the Cu–Zn combinatorial library on various positions on the sample.

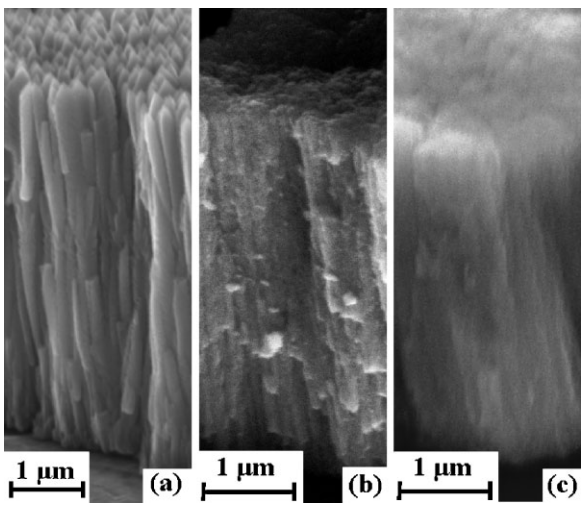

Figure 5 SEM image of the cross-section of the Cu–Zn thin film oxide alloys for various compositions, (a) Cu–1.5 at.% Zn, (b) Cu–25.4 at.% Zn, and (c) Cu-53.7 at.% Zn.

this is shown for Cu–54 at.% Zn where, even though a columnar structure can still be observed, a clear separation between the columns is almost impossible to be detected.

The crystallographic properties of the Cu–Zn thin film oxide alloys were investigated using scanning XRD (SXRD). Diffraction patterns were recorded at various positions on the surface of the combinatorial library associated to certain compositions through the XRF mapping previously presented in Fig. 2. A few SXRD spectra representing each of the identified compositional zones are shown in Fig. 6 together with a spectrum measured on uncoated substrate. The composition of each alloy is given near each spectrum shown in Fig. 6. The first two spectra from the top of the graph, measured for alloys up to 8 at.% Zn have similar features describing the first compositional zone. Here, only the presence of Cu_2O and CuZn intermetallics was found.

This indicates that the Zn present in the alloys of the first compositional zone appears only in the CuZn intermetallics, while the Cu appears also in its oxidized form. Increasing the amount of Zn in the Cu–Zn compositional spread, in the second zone previously identified, the presence of pure Cu could be observed. The next two spectra presented in Fig. 6 reaching more than 29 at.% Zn are representative for this region. The CuZn intermetallics and Cu_2O are still present together with a Cu (111) peak whose intensity increases with the amount of Zn. Starting the third compositional zone, the pure Cu peak disappears together with the Cu_2O while the CuZn (110) peak decreases in intensity and eventually vanishes for Zn concentrations higher than 62 at.%. The third compositional zone is mainly characterized by the presence of ZnO, a weak Cu (111) peak being observable for alloys containing around 45 at.% Zn.

In order to investigate the in-depth composition of the Cu–Zn thin film oxide alloy combinatorial library, XPS depth profiling was used. The depth profiles corresponding to Cu and O are presented in Fig. 7a and b, respectively, for various alloys within the Cu–Zn compositional spread. The Zn profiles are complementary to the ones belonging to Cu and O. The first compositional zone can be identified in the

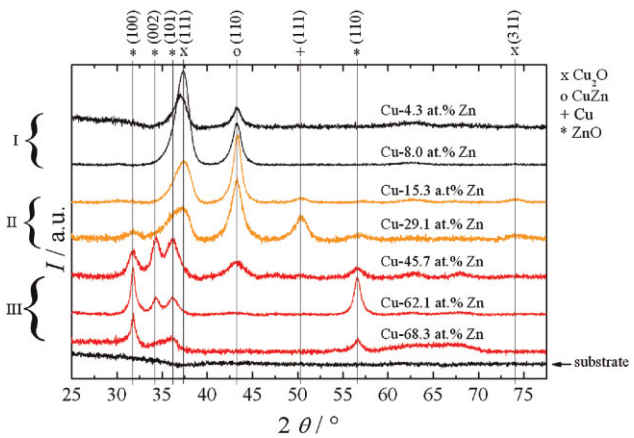

Figure 6 XRD spectra of selected compositions on the surface of the Cu–Zn thin film oxide alloy library.

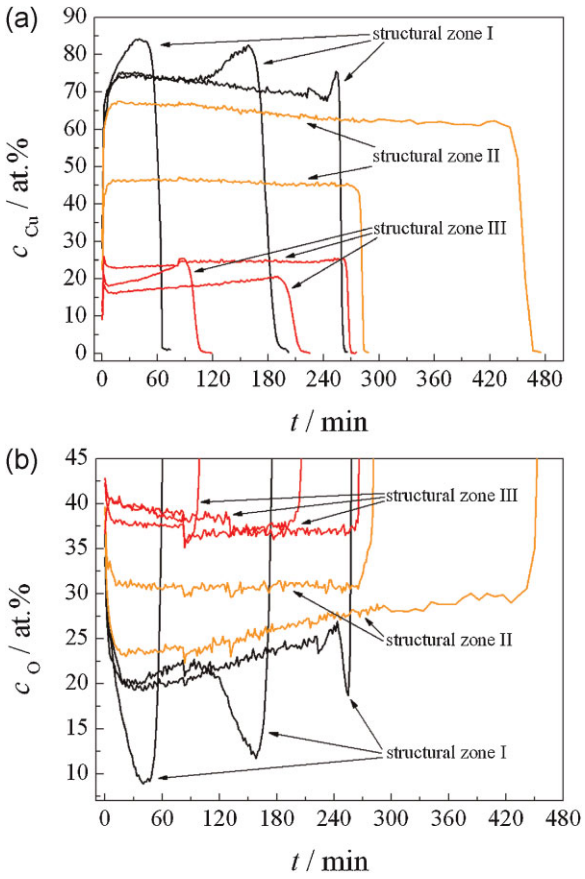

Figure 7 (a) XPS depth profile of the Cu–Zn thin film oxide alloys for various compositions showing the in-depth Cu concentration depending on the XPS sputter time *t*. (b) XPS depth profile of the Cu–Zn thin film oxide alloys for various compositions showing the in-depth Cu concentration depending on the XPS sputter time *t*.

depth profiles at the highest Cu concentrations. In this zone, a Cu enrichment close to the film/substrate interface can be observed for the three top-most XPS curves from Fig. 7a. Combining this observation with the crystallographic characterization from Fig. 6 it can be concluded that the CuZn intermetallic is accumulating at the interface. This is also observed in the oxygen spectra from Fig. 7b, where three oxygen decays can be observed for the two bottom-most curves confirming the presence of a metallic state. The other two compositional zones showed no metallic separation in-depth of the Cu–Zn thin oxide films. Both regions have a similar behaviour, the Cu and Zn content remaining almost constant in-depth of the films. Overall, increasing the Zn concentration has led to an increase in the O concentration while the Cu amount decreases. This behaviour correlates well with the XRD measurements from Fig. 6 and they show a preferential ZnO formation in the second and third previously identified compositional zones.

4 Conclusions In the present work the preparation and characterization of Cu–Zn oxide thin films fabricated by reactive co-sputter deposition using a sectioned two-

component metallic target is presented. A Cu–Zn compositional spread was characterized together with a thickness gradient, defining a combinatorial library. The microstructure of the Cu–Zn thin films oxide alloys was analyzed by SEM and three compositional zones with structural differences could be identified. XRD investigations have revealed different crystalline structures for each of the three zones. CuZn intermetallics and pure Cu-phase were identified together with Cu_2O and ZnO. XPS depth profiles have shown a metallic phase segregation at the thin film/substrate interface for the first compositional zone while an increased tendency of ZnO formation was identified at higher Zn concentrations. This finding can be related to the higher oxygen affinity of Zn compared to Cu.

Acknowledgements The authors gratefully acknowledge assistance in XPS measurements by Jiri Duchoslav (ZONA).

References

[1] J. A. Thornton, J. Vac. Sci. Technol. A **4**, 3056–3059 (1986).
[2] H. Savaloni and S. B. Najmi, Vacuum **66**, 49–58 (2002).
[3] R. Ondo-Ndong, F. Pascal-Delannoy, A. Boyer, A. Giani, and A. Foucaran, Mater. Sci. Eng. B **97**, 68–73 (2003).
[4] H. Czternastek, Opto-Electon. Rev. **12**, 49–52 (2004).
[5] Z. Li and W. Gao, Mater. Lett. **58**, 1363–1370 (2003).
[6] C. Besleaga, G. Stan, A. Galca, L. Ion, and S. Antohe, Appl. Surf. Sci. **258**, 8819–8824 (2012).
[7] S. Badadhe and I. Mulla, Sens. Actuators B **143**, 164–170 (2009).
[8] Y.-S. Chang and J.-M. Ting, Thin Solid Films **398–399**, 29–34 (2001).
[9] M. Goto, A. Kasahara, and M. Tosa, Appl. Surf. Sci. **252**, 2482–2487 (2006).
[10] C.-L. Chu, H.-C. Lu, C.-Y. Lo, C.-Y. Lai, and Y.-H. Wang, Physica B **404**, 4831–4834 (2009).
[11] C. Azana Ricardo, M. D'Incau, M. Leoni, C. Malerba, A. Mittiga, and P. Scardi, Thin Solid Films **520**, 280–286 (2011).
[12] A. Kostruba, B. Kulyk, and B. Turko, J. Alloys Compd. **518**, 96–100 (2012).
[13] L. Ma, S. Ma, H. Chen, X. Ai, and X. Huang, Appl. Surf. Sci. **257**, 10036–10041 (2011).
[14] N.-E. Sung, I.-J. Lee, A. Thakur, K. H. Chae, H.-J. Shin, and H.-K. Lee, Mater. Res. Bull. **47**, 2891–2894 (2012).
[15] X. Peng, J. Xu, H. Zang, B. Wang, and Z. Wang, J. Lumin. **128**, 297–300 (2008).
[16] H. Gong, J. Q. Hu, J. H. Wang, C. H. Ong, and F. R. Zhu, Sens. Actuators B **115**, 247–251 (2006).
[17] A. I. Mardare, A. Ludwig, A. Savan, A. D. Wieck, and A. W. Hassel, Electrochim. Acta **55**, 7884–7891 (2010).
[18] A. I. Mardare, A. Ludwig, A. Savan, A. D. Wieck, and A. W. Hassel, Electrochim. Acta **54**, 5171–5178 (2009).
[19] A. I. Mardare, A. Savan, A. Ludwig, A. D. Wieck, and A. W. Hassel, Corros. Sci. **51**, 1519–1527 (2009).
[20] S. O. Klemm, J. P. Kollender, and A. W. Hassel, Corros. Sci. **53**, 1–6 (2011).
[21] Z. Wronski and J. Sielanko, Vacuum **78**, 605–610 (2005).
[22] S. O. Klemm, A. G. Martin, J. Lengsfeld, J. C. Schauer, B. Schuhmacher, and A. W. Hassel, Phys. Status Solidi **207**, 801–806 (2010).